J. Fluid Mech. (1984), *vol.* 149, *pp.* 403–429
Printed in Great Britain

A linearized unsteady aerodynamic analysis for transonic cascades

By JOSEPH M. VERDON AND JOSEPH R. CASPAR
United Technologies Research Center, East Hartford, Connecticut 06108

(Received 24 February 1984 and in revised form 6 June 1984)

A linearized potential-flow analysis is presented for predicting the unsteady airloads produced by the vibrations of turbomachinery blades operating at transonic Mach numbers. The unsteady aerodynamic model includes the effects of blade geometry, non-zero mean-pressure variation across the blade row, high-frequency blade motion, and shock motion within the framework of a linearized frequency-domain formulation. The unsteady equations are solved using an implicit least-squares finite-difference approximation which is applicable on arbitrary grids. A numerical solution for the entire unsteady flow field is determined by matching a solution determined on a rectilinear-type cascade mesh, which covers an extended blade-passage region, to a solution determined on a detailed polar-type local mesh, which covers and extends well beyond the supersonic region(s) adjacent to a blade surface. Results are presented for cascades of double-circular-arc and flat-plate blades to demonstrate the unsteady analysis and to partially illustrate the effects of blade geometry, inlet Mach number, blade-vibration frequency and shock motion on unsteady response.

1. Introduction

At transonic Mach numbers relatively small-amplitude unsteady motions can produce large variations in the magnitude and phase of the aerodynamic forces and moments. These characteristics enhance the likelihood of an aeroelastic instability and thus are a major concern in transonic design. Of particular concern are flutter boundaries. The aeroelastician is normally confronted with determining the stability of a configuration with respect to infinitesimal disturbances. For this purpose a linearized unsteady aerodynamic theory is desirable. Although substantial progress has been achieved towards the development of both linear and nonlinear unsteady transonic theories for fixed wings (as reviewed by Tijdeman & Seebass 1980), these are either too restrictive or too expensive to permit their routine use in detailed turbomachinery aeroelastic investigations. Thus the objective of the present effort is to provide a linearized unsteady transonic analysis for two-dimensional cascades which accounts for the effects of blade geometry and loading and applies at high vibration frequency. Although the attention here is focused on turbomachinery applications, the basic aerodynamic model described in this paper could also lead to useful methods for predicting the unsteady loads associated with the motions of a variety of aerodynamic configurations including those of thick, blunt-nosed, transonic airfoils.

The unsteady aerodynamic models currently used for turbomachinery aeroelastic design predictions (for an informative review see Whitehead 1980) are essentially based on classical linearized theory. Here both steady and unsteady disturbances caused by airfoil shape and incidence and by airfoil motion respectively are regarded

as being of the same order of magnitude and small relative to the free-stream speed, leading to linear constant-coefficient boundary-value problems for the steady and unsteady disturbance potentials. The classical formulation admits very efficient semianalytic solutions for entirely subsonic or entirely supersonic flows, and it has recently been extended by Goldstein, Braun & Adamczyk (1977) to provide solutions for flows in supersonic cascades with strong in-passage shocks. However, this formulation does not account for interactions between the steady and unsteady disturbances, and such interactions are believed to be crucial to the successful prediction of unsteady transonic airloads as well as to the understanding of a variety of turbomachinery aeroelastic phenomena. The influence of steady disturbances on unsteady response is retained in the so called 'time-linearized' transonic small-disturbance approximation. Here unsteady disturbances are regarded as small relative to steady disturbances caused by airfoil shape and incidence, which are in turn assumed to be small relative to the free-stream speed. These assumptions along with appropriate independent-variable scalings provide a linearized theory which formally applies at free-stream Mach numbers close to one, but only for low-frequency unsteady motions. Finite-difference methods have been developed for solving the time-linearized transonic equations in either the time (Fung, Yu & Seebass 1978) or frequency (Ehlers & Weatherill 1982) domain. But these methods have been applied only to the prediction of unsteady transonic flows around isolated airfoils.

The flat mean-surface approximation, used in the treatment of airfoil and wake boundary conditions, is an important simplification associated with the foregoing linearized unsteady models. However, the assumptions that permit this simplification place severe restrictions on airfoil geometry and loading and, in the transonic case, on the frequency of the unsteady motion. As such, these theories fail to meet the needs of turbomachinery designers over a wide range of practical operating conditions. To partially overcome the foregoing limitations, linearized unsteady aerodynamic models have recently been formulated for subsonic cascades which include the effects of blade geometry and loading on unsteady response (Atassi & Akai 1978; Verdon & Caspar 1980; Whitehead & Grant 1981; Caruthers 1981). Here the unsteady flow is regarded as a small-amplitude harmonic fluctuation about a fully non-uniform steady flow. The steady flow is determined as a solution of the full potential equation, and the unsteady flow is governed by a linear equation with variable coefficients which depend on the underlying steady flow. Several accurate and reliable numerical solution algorithms for the nonlinear steady problem are currently available (see McNally & Sockol 1981). In addition, a finite-difference approximation based on an implicit least-squares development and applicable on arbitrary grids has been developed by the present authors for resolving the linearized subsonic unsteady problem (Caspar & Verdon 1981). Numerical results have been reported for vibrating cascades of sharp-edged, double-circular-arc and thin-circular-arc airfoils and for cascades of blunt-nosed NACA 0012 (Verdon & Caspar 1982) and NACA 65 series airfoils. Predictions for the NACA 65 series airfoils were found to be in excellent agreement with cascade wind-tunnel measurements made by Carta (1983).

In the present effort the aerodynamic and numerical models developed previously by the present authors (1980, 1981, 1982) have been extended for transonic applications. This has been accomplished by introducing shock-jump conditions into the linearized unsteady formulation and by including the concentrated loads produced by shock motion in the determination of unsteady force and moment. In addition, transonic differencing strategies and shock-fitting procedures have been incorporated into the unsteady numerical approximation. This approximation has

been implemented on both cascade and local meshes. The latter is required to resolve the flow accurately in supersonic regions and to fit shocks into the unsteady solution. In this paper the unsteady transonic aerodynamic model and numerical approximation are described, and numerical results are presented and evaluated for cascades of vibrating sharp-edged double-circular-arc (DCA) airfoils. This simple example configuration has been selected to permit concentration on the transonic aspects of the unsteady problem (i.e. local supersonic regions and moving shocks) without introducing the additional complications associated with rounded blade edges and mean incidence.

The concept of linearizing unsteady fluctuations with respect to a fully non-uniform mean flow has been employed in other unsteady aerodynamic applications; e.g. in studies on turbulent flows past obstacles (see Hunt 1973; Goldstein 1979). However, with the exception of the subsonic cascade analyses referred to above and the present transonic cascade analysis, this concept has not been widely exploited for developing unsteady analyses intended for aeroelastic applications. The improvements in physical modelling offered by such a linearization coupled with advances in our ability to resolve the resulting governing equations numerically should make this approach an increasingly attractive one for future consideration.

2. Problem description and governing equations

In the following discussion all physical quantities are dimensionless. Lengths have been scaled with respect to blade chord, time with respect to the ratio of blade chord to upstream free-stream speed, and density and pressure with respect to the upstream free-stream density and dynamic pressure respectively. We consider adiabatic flow, with negligible body forces, of an inviscid non-heat-conducting perfect gas through a two-dimensional oscillating cascade (see figure 1). The mean or steady-state positions of the blade chord lines coincide with the line segments $\eta = \xi \tan\Theta + m|\boldsymbol{G}|$, $0 \leqslant \xi \leqslant \cos\Theta$, $m = 0, \pm 1, \pm 2, \ldots$, where ξ and η are the cascade axial and circumferential coordinates, m is a blade-number index, Θ is the cascade stagger angle, and $\boldsymbol{G}$ is the cascade gap vector, which is directed along the η-axis with magnitude equal to the blade spacing. It is assumed that in the absence of blade motions uniform subsonic conditions exist far upstream and downstream of the blade row. The blades are undergoing identical harmonic motions at frequency ω and with constant phase angle σ between the motion of adjacent blades. Blade shape and orientation relative to the inlet free stream and the amplitude, frequency and mode of the blade motion are assumed to be such that the flow remains attached to the blade surfaces. Thus thin vortex sheets (unsteady wakes) emanate from the blade trailing edges and extend downstream. In addition, for sufficiently high subsonic inlet conditions local supersonic regions which terminate at moving shocks will appear adjacent to blade surfaces.

2.1. *Time-dependent full potential formulation*

Equations governing the fluid motion can be derived from the integral conservation laws for mass, momentum and energy, and the thermodynamic relations for a perfect gas. The former provide corresponding differential equations in regions where the flow variables are continuously differentiable and 'jump' conditions at surfaces across which (in the inviscid approximation) the flow variables are discontinuous, i.e. at shocks and blade wakes. In continuous regions the energy equation can be replaced by the requirement that the entropy following a fluid particle must remain constant

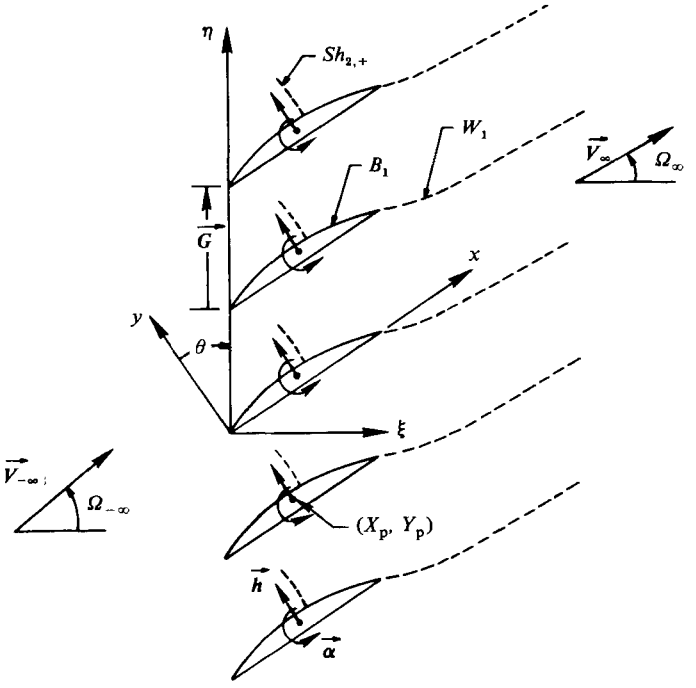

FIGURE 1. Two-dimensional oscillating transonic cascade with mean-flow deflection.

(see Aris 1962). In general, the discontinuous changes in the flow quantities across a shock are proportional to the shock strength, but the change in entropy is proportional only to the third power of the shock strength (see Whitham 1974). Thus for a shock of weak to moderate strength it is a reasonable approximation to neglect changes in entropy across the shock. With this approximation the uniform undisturbed flow far upstream of the cascade will produce an isentropic and hence, by the Helmholtz theorem, an irrotational, time-dependent flow.

The mass-conservation law then provides the following differential equation governing the fluid density $\hat{\rho}$ and velocity potential $\hat{\Phi}$:

$$\frac{\partial \hat{\rho}}{\partial t} + \nabla \cdot (\hat{\rho} \nabla \hat{\Phi}) = 0, \tag{2.1}$$

where t is time. In addition, after substituting the isentropic relations into the differential form of the momentum conservation law and integrating the resulting expression, it follows that

$$\hat{\rho}^{\gamma-1} = (\tfrac{1}{2}\gamma M_{-\infty}^2 \hat{P})^{(\gamma-1)/\gamma} = (M_{-\infty} \hat{A})^2 = 1 - (\gamma - 1) M_{-\infty}^2 \{\hat{\Phi}_t + \tfrac{1}{2}((\nabla \hat{\Phi})^2 - 1)\}. \tag{2.2}$$

Here γ is the specific-heat ratio of the fluid, M is the Mach number of the undisturbed or steady flow, $\hat{P}$ is the fluid pressure, $\hat{A}$ is the speed of sound propagation and the subscript $-\infty$ refers to the upstream free-stream condition. Since, by assumption, unsteady disturbances are produced solely by the blade motion, the admissible solutions of (2.1) and (2.2) for the present application are those in which acoustic energy does not radiate towards the blade row. Blade motions are then classified as subresonant if all acoustic waves attenuate in the far field; as superresonant if at least one such wave persists in the far field and carries energy away from the blade row in either the far-upstream or downstream axial direction; or as resonant if acoustic energy persists in the far field but is carried only in the circumferential direction.

The foregoing equations are supplemented by boundary conditions on moving blade surfaces $\mathscr{B}_m$, and jump conditions at moving blade wakes $\mathscr{W}_m$ and at moving shocks $\mathscr{S}\!h_{m,+}$, where the subscript + or − refers to a shock emanating from the upper or lower surface, respectively, of the mth blade. Note that we use italic letters to denote the mean on steady-state surface positions as shown in figure 1. The vectors $\mathscr{R}$, $\boldsymbol{n}$, and $\boldsymbol{\tau}$ are introduced below in conjunction with the surface conditions. The relative-displacement vector $\mathscr{R}$ measures the displacement of a point on the instantaneous position of a surface (blade, wake or shock) relative to its mean or steady-state position. The unit vectors $\boldsymbol{n}$ and $\boldsymbol{\tau}$ are normal and tangent, respectively, to a surface and directed such that $\boldsymbol{n}\times\boldsymbol{\tau}=\boldsymbol{e}_z$ points out from the page. The unit normal vector is directed outward from blade surfaces, upward at wakes, and downstream at shocks.

For attached flows the normal component of the fluid velocity must equal the normal component of the surface velocity at blade surfaces (flow tangency), i.e.

$$\nabla\hat{\Phi}\cdot\boldsymbol{n}=\frac{\partial\mathscr{R}}{\partial t}\cdot\boldsymbol{n}\quad\text{on }\mathscr{B}_m, \tag{2.3}$$

where the vector $\mathscr{R}$ is prescribed. The blade wakes are also material surfaces; i.e. a fluid particle on the wake always remains there. Hence (2.3) also applies at wake surfaces. However, since the wake displacement vector is unknown *a priori*, an additional wake condition is required. This follows from the foregoing kinematic condition and the integral form of the mass-conservation law and requires that the density, and hence the thermodynamic properties, of the fluid must be continuous across thin vortex wakes. Thus the conditions

$$[\![\nabla\hat{\Phi}]\!]\cdot\boldsymbol{n}=[\![\hat{P}]\!]=0\quad\text{on }\mathscr{W}_m \tag{2.4}$$

apply at wake surfaces, where $[\![\ ]\!]$ denotes the difference (upper minus lower) in a quantity across a wake.

At shocks the mass-conservation law requires that

$$\left[\!\!\left[\hat{\rho}\left(\nabla\hat{\Phi}-\frac{\partial\mathscr{R}}{\partial t}\right)\right]\!\!\right]\cdot\boldsymbol{n}=0\quad\text{on }\mathscr{S}\!h_{m,\pm}, \tag{2.5}$$

where $[\![\ ]\!]$ denotes the jump or difference (downstream minus upstream) in quantity across a shock. A second shock-jump condition follows from the conservation of momentum tangential and requires that the component of fluid velocity tangent to a shock or, after integrating along the shock, that the velocity potential must be continuous across a shock; i.e.

$$[\![\hat{\Phi}]\!]=0\quad\text{on }\mathscr{S}\!h_{m,\pm}. \tag{2.6}$$

Equation (2.6) also represents the requirement that no vorticity be produced at a shock. In the potential approximation the conservation laws (see Whitham 1974, p. 171) for the normal component of fluid momentum and for the fluid energy (internal plus kinetic) are not imposed at shocks; as these are essentially precluded by the isentropic assumption. Thus in the present formulation neither the normal component of fluid momentum nor energy will be conserved across a shock.

The formulation of the boundary-value problem for the velocity potential $\hat{\Phi}$ is now complete. The problem posed is a formidable one consisting of a nonlinear time-dependent partial differential equation along with conditions imposed on moving blade, shock and wake surfaces in which the instantaneous locations of shock and wake surfaces must, in principle, be determined as part of the solution. Although numerical solutions to this problem would be of substantial interest, they would be

of limited practical value because of the prohibitive expense involved in obtaining the detailed unsteady response predictions required for turbomachinery flutter calculations. Thus in the present effort we will derive an approximation to the foregoing boundary-value problem, which is valid for small-amplitude (infinitesimal) blade motions, with the intention of providing a useful analytical model for turbomachinery aeroelastic investigations.

3. The small-unsteady disturbance approximation

3.1. *Linearization*

We will seek an approximate solution to the foregoing time-dependent boundary value problem for small-amplitude (i.e. $|\mathscr{R}| = O(\epsilon) \ll 1$) blade motions. For this purpose the flow variables are first expanded in an asymptotic series in ϵ, e.g.

$$\hat{\Phi}(\boldsymbol{X}, t) = \phi_0(\boldsymbol{X}) + \epsilon\phi_1(\boldsymbol{X}, t) + O(\epsilon^2), \tag{3.1}$$

where $\boldsymbol{X}$ is a position vector referred to the space-fixed (x, y) Cartesian coordinate frame of figure 1. In addition, Taylor-series expansions, e.g.

$$\nabla\hat{\Phi}|_{\mathscr{S}} = \nabla\hat{\Phi}|_S + (\mathscr{R}\cdot\nabla)\nabla\hat{\Phi}|_S + O(\epsilon^2), \tag{3.2}$$

are applied to refer information at a moving blade, wake or shock surface to the mean position of this surface. In (3.2) the subscripts $\mathscr{S}$ and S refer to the instantaneous and mean surface locations respectively. Unit tangent and normal vectors at a point on a moving surface are related to the unit tangent and normal vectors at the location of this point on the mean surface as follows:

$$\boldsymbol{\tau}_{\mathscr{S}} = [1 - \boldsymbol{\tau}_S\cdot\nabla\mathscr{R}\cdot\boldsymbol{\tau}_S]\,\boldsymbol{\tau}_S + (\boldsymbol{\tau}_S\cdot\nabla)\,\mathscr{R} + O(\epsilon^2) \tag{3.3}$$

and

$$\boldsymbol{n}_{\mathscr{S}} = \boldsymbol{\tau}_{\mathscr{S}} \times \boldsymbol{e}_z = [1 - \boldsymbol{\tau}_S\cdot\nabla\mathscr{R}\cdot\boldsymbol{\tau}_S]\,\boldsymbol{n}_S + (\boldsymbol{\tau}_S\cdot\nabla)\,\mathscr{R} \times \boldsymbol{e}_z + O(\epsilon^2). \tag{3.4}$$

After substituting the foregoing series expansions and surface-vector relations into the full governing equations, equating terms of like power in ϵ and neglecting terms of second and higher order in ϵ, nonlinear and linear variable-coefficient boundary-value problems are obtained respectively for the zeroth- and first-order flows.

The zeroth-order term $\phi_0(\boldsymbol{X})$ in (3.1) is the velocity potential $\Phi(\boldsymbol{X})$ due to steady flow past a stationary cascade. Equations governing this steady flow, which is assumed to be known in the present study, follow from (2.1) through (2.6) after replacing the time-dependent flow properties $\hat{\Phi}$, $\hat{P}$, $\hat{\rho}$ and $\hat{A}$ by their zeroth-order or steady-flow counterparts, Φ, P, $\bar{\rho}$ and A, setting temporal derivatives equal to zero, and imposing the resulting surface conditions at the blade, wake and shock mean positions. Since the first-order or unsteady problem is linear, the first-order potential We take advantage of this feature by introducing a complex representation, e.g. $\epsilon\phi_1(\boldsymbol{X}, t) = \phi(\boldsymbol{X})\,\mathrm{e}^{\mathrm{i}\omega t}$, for all first-order flow variables, including the surface-displacement vectors, and adopting the convention that the real parts of these complex parameters represent the actual time-dependent physical quantities. The complex representation serves to remove explicit time dependence from the linearized unsteady problem, thereby facilitating the determination of a solution. In addition, the cascade geometry, the prescribed form of the blade motion, i.e.

$$\mathscr{R}(\boldsymbol{X} + m\boldsymbol{G}, t) = \boldsymbol{r}(\boldsymbol{X})\,\mathrm{e}^{\mathrm{i}(\omega t + m\sigma)} \quad \text{for } \boldsymbol{X} \text{ on } B, \tag{3.5}$$

where $\mathscr{R}$ is now a complex displacement vector and the vector $\boldsymbol{r}$ defines the amplitude and direction of the reference blade displacement, and the linearity of the first-order problem require that the unsteady flow exhibit blade-to-blade periodicity, i.e.

$$\phi(\boldsymbol{X}) = \phi(\boldsymbol{X} + m\boldsymbol{G})\,\mathrm{e}^{-\mathrm{i}m\sigma}, \tag{3.6}$$

and that (3.5) also apply to shock and wake displacements. The periodicity condition (3.6) allows a numerical resolution of the unsteady flow to be limited to a single extended blade-passage region of the cascade and permits properties at the mth blade, wake or shock surface to be evaluated in terms of information provided at the corresponding reference ($m = 0$) surface. For simplicity, the subscript m will be omitted in the following discussion when referring to a reference surface.

It must be noted that the foregoing linearization is not valid in the immediate neighbourhood of a moving shock (see Hounjet 1981). An observer situated between the extreme shock positions will experience large-amplitude jumps in the flow variables as the shock passes by. Such local anharmonic effects can be accounted for by including additional terms in the asymptotic representations of the flow variables (see Williams 1979). However, since these have no impact on the linearized unsteady boundary-value problem, we defer their introduction until the subsequent discussion on unsteady aerodynamic response.

3.2. *The linearized unsteady boundary-value problem*

It follows from the differential form of the mass-conservation law (2.1), the Bernoulli relations (2.2) and the asymptotic expansions for the flow variables (3.1), that the linearized unsteady flow is governed by the field equation

$$\mathrm{i}\omega\rho + \boldsymbol{\nabla}\cdot[\bar{\rho}\boldsymbol{\nabla}\phi + \rho\boldsymbol{\nabla}\boldsymbol{\Phi}] = 0, \tag{3.7}$$

and that the complex amplitudes of the first-harmonic unsteady density ρ, pressure p, speed of sound a and velocity potential ϕ are related by

$$\frac{\rho}{\bar{\rho}} = \gamma^{-1}\frac{p}{P} = \frac{2}{\gamma-1}\frac{a}{A} = -A^{-2}\frac{\mathrm{D_S}\phi}{\mathrm{D}t}, \tag{3.8}$$

where $\mathrm{D_S}/\mathrm{D}t = \mathrm{i}\omega + \boldsymbol{\nabla}\boldsymbol{\Phi}\cdot\boldsymbol{\nabla}$ is a mean-flow convective-derivative operator. Upon substituting the steady and linearized unsteady (3.8) Bernoulli relations into (3.7) and performing some algebra, the following non-conservative form of the field equation for the unsteady potential is obtained:

$$A^2\nabla^2\phi = \frac{\mathrm{D_S^2}\phi}{\mathrm{D}t^2} + (\gamma-1)\nabla^2\boldsymbol{\Phi}\frac{\mathrm{D_S}\phi}{\mathrm{D}t} + \tfrac{1}{2}\boldsymbol{\nabla}(\boldsymbol{\nabla}\boldsymbol{\Phi})^2\cdot\boldsymbol{\nabla}\phi. \tag{3.9}$$

Conditions on the unsteady flow at blade B_m, wake W_m and shock $Sh_{m,\pm}$ mean positions are obtained similarly by substituting the asymptotic (3.1) and Taylor (3.2) series expansions and the surface-vector relations (3.3) and (3.4) into the time-dependent flow-tangency (2.3), wake-jump (2.4) and shock-jump (2.5) and (2.6) conditions. After performing some straightforward algebra, the following conditions on the linearized unsteady flow are determined. The first-order flow tangency condition has the form

$$\boldsymbol{\nabla}\phi\cdot\boldsymbol{n} = [\mathrm{i}\omega\boldsymbol{r} + (\boldsymbol{\nabla}\boldsymbol{\Phi}\cdot\boldsymbol{\tau})(\boldsymbol{\tau}\cdot\boldsymbol{\nabla})\boldsymbol{r} - (\boldsymbol{r}\cdot\boldsymbol{\nabla})\boldsymbol{\nabla}\boldsymbol{\Phi}]\cdot\boldsymbol{n} \quad \text{on } B_m. \tag{3.10}$$

Since the steady velocity and pressure are continuous downstream of the blade row, the conditions of continuity of normal velocity and pressure across blade wakes reduce simply to

$$[\![\boldsymbol{\nabla}\phi]\!]\cdot\boldsymbol{n} = \left[\!\!\left[\frac{\mathrm{D_S}\phi}{\mathrm{D}t}\right]\!\!\right] = 0, \quad \text{on } W_m, \tag{3.11}$$

where the wake mean positions W_m are assumed to coincide with the downstream steady-flow stagnation streamlines. At shocks, conservation of mass and tangential momentum require that

$$\left[\mathrm{i}\omega r_n + \boldsymbol{\Phi}_\tau\frac{\partial r_n}{\partial\tau}\right][\![\bar{\rho}]\!] = [\![\bar{\rho}\boldsymbol{\nabla}\phi + \rho\boldsymbol{\nabla}\boldsymbol{\Phi}]\!]\cdot\boldsymbol{n} + r_n[\![(\bar{\rho}\boldsymbol{\Phi}_n)_n]\!] \quad \text{on } Sh_{m,\pm} \tag{3.12}$$

and
$$[\![\phi]\!] + r_n [\![\Phi_n]\!] = 0 \quad \text{on } Sh_{m,\pm} \tag{3.13}$$

respectively, where $r_n = \mathscr{R} \cdot \boldsymbol{n}$ is the complex amplitude of the shock displacement normal to the mean shock locus and the subscripts on Φ denote partial derivatives in the indicated directions. For normal shocks $\Phi_\tau|_{Sh}$ and $[\![(\bar{\rho}\Phi_n)_n]\!]$ are identically zero. It therefore follows from (3.8), (3.12) and (3.13) and some algebra that the unsteady potential must satisfy the jump condition

$$\mathrm{i}\omega[\![([\![\bar{\rho}]\!] - M_{-\infty}^2 \bar{\rho}^{2-\gamma} \Phi_n [\![\Phi_n]\!])\phi]\!] = [\![\Phi_n]\!] [\![\bar{\rho}(M_{-\infty}^2 \bar{\rho}^{1-\gamma} \Phi_n^2 - 1)\phi_n]\!] \quad \text{on } Sh_{m,\pm}, \tag{3.14}$$

where $\bar{\rho}$, Φ and the mean shock locations $Sh_{m,\pm}$, are assumed to be known from the steady solution. Equations (3.14) and (3.13) provide the required relations for determining the jump in the unsteady potential at the mean location of a normal shock and the complex amplitude of the shock displacement in the streamwise direction respectively. The latter quantity is required to determine the concentrated loads produced by shock motion.

Under uniform mean subsonic inlet and exit conditions the departure of steady flow quantities from their free-stream values will be $O(\epsilon)$ beyond some finite distances upstream and downstream from the blade row. Thus in the far field and to within the first-order approximation considered here, the unsteady differential equation (3.7) can be reduced to the familiar constant-coefficient equation of classical linearized theory. The unsteady potential is continuous upstream of the blade row and has both a continuous and discontinuous component downstream. The continuous component accounts for acoustic wave propagation and the discontinuous component accounts for counter vorticity shed from the blade trailing edges and convected along the blade wakes. Analytic far-field solutions for the continuous and discontinuous components of the unsteady potential have been determined (see Verdon & Caspar 1980) which can be matched to a near-field numerical solution, and thus serve to complete the specification of the linearized unsteady boundary value problem.

4. Aerodynamic response coefficients

4.1. *Surface-pressure distributions*

A solution to the linearized unsteady boundary-value problem is required to determine unsteady surface-pressure distributions and global unsteady airloads. The latter are the important results of an aerodynamic analysis intended for flutter prediction, since they permit the evaluation of aerodynamic work per cycle and/or aerodynamic damping; either of which can be used to determine whether the airstream tends to support or suppress a prescribed blade motion. The pressure acting at the instantaneous position of the mth blade surface is given by

$$\hat{P}_{\mathscr{B}m}(\tau, t) = P_B(\tau) + \mathrm{Re}\{p_{\mathscr{B}}(\tau)\, \mathrm{e}^{\mathrm{i}(\omega t + m\sigma)}\} + p_{\mathscr{S}\!h_{m,+}}(\tau, t) + p_{\mathscr{S}\!h_{m,-}}(\tau, t) + \ldots, \tag{4.1}$$

where τ is a coordinate measuring distance in the counter-clockwise direction along the mean blade surface. The first two terms on the right-hand side of (4.1) are the steady and first-harmonic components of the pressure acting at the mth moving blade surface outside the small intervals bounded by the mean and instantaneous shock locations. The third and fourth terms represent the anharmonic contributions to the unsteady surface pressure caused by the motion of the shocks along the upper and lower surfaces of the mth blade.

After expanding the pressure $\hat{P}$ in the manner indicated by (3.1) and (3.2), it follows

from the steady and unsteady Bernoulli relations that the first harmonic component of the pressure acting at a moving blade surface $\mathscr{B}_m$ can be evaluated in terms of information supplied at the mean position B of the reference blade; i.e.

$$p_{\mathscr{B}} = \left[-2(M_{-\infty} A)^{2/(\gamma-1)} \frac{\mathrm{D_S}\phi}{\mathrm{D}t} + (\boldsymbol{r}\cdot\boldsymbol{\nabla}) P \right]_B. \tag{4.2}$$

The first term of the right-hand side of (4.2) is the harmonic unsteady pressure at the mean position of the reference blade, and the second is the harmonic surface pressure produced by motion through a spatially varying steady pressure field.

Following Williams (1979), the local anharmonic effect caused by shock motion is accounted for by assuming that

$$p_{\mathscr{S}\!h}(\tau, t) = -\frac{\mathrm{Re}\{r_n(0)\}}{|\mathrm{Re}\{r_n(0)\}|} H[(\tau-\tau_{Sh})(\tau_{\mathscr{S}\!h}-\tau)]\, Q(\tau, t), \tag{4.3}$$

where $r_n(0)$ is the displacement of the shock foot along the blade surface, H is the unit step function and

$$Q(\tau, t) = [\![P_B]\!] + (\tau-\tau_{Sh}) \left[\!\!\left[\frac{\partial P_B}{\partial \tau}\right]\!\!\right] + \mathrm{Re}\,\{[\![p_{\mathscr{B}}]\!] \mathrm{e}^{\mathrm{i}(\omega t + m\sigma)}\}. \tag{4.4}$$

The first two terms on the right-hand side of (4.1) are discontinuous at the undisturbed shock locations. The third and fourth terms cancel these discontinuities and transfer them to the instantaneous shock locations. This can be seen by setting $\tau = \tau_{\mathscr{S}\!h}{}^{\pm}$ in the foregoing equations to determine an expression for $[\![\hat{P}_{\mathscr{B}}]\!]$ at the instantaneous shock location. Although the unsteady pressure disturbance is not everywhere harmonic, its regions of anharmonicity are small. Consequently (see Tijdeman 1977; Ehlers & Weatherill 1982) the first-order global aerodynamic coefficients are harmonic in time.

4.2. *Unsteady force and moment*

Up to this point we have placed no restriction on the mode of the blade motion. But we now limit consideration to the case usually considered in turbomachinery flutter calculations wherein each incremental blade section is undergoing a rigid-body motion. In this case only the unsteady force and moment coefficients must be determined to analyse the stability of the blade motion. For rigid blade motions the first-order displacement-amplitude vector is given by

$$\boldsymbol{r}(\boldsymbol{X}) = \boldsymbol{h} + \boldsymbol{a} \times \boldsymbol{R}_{\mathrm{p}} \quad \boldsymbol{X} \text{ on } B, \tag{4.5}$$

where $\boldsymbol{h}$ defines the amplitude and direction of blade translations, $\boldsymbol{a}$ defines the amplitude and direction (positive counterclockwise) of blade rotations and $\boldsymbol{R}_{\mathrm{p}}$ is a position vector extending from the mean position of the reference blade axis of rotation (i.e. from the point $(X_{\mathrm{p}}, Y_{\mathrm{p}})$) to points on the mean position of the reference blade surface. These rigid two-dimensional motions model bending and torsional vibrations of actual rotor blades. The components h_x, h_y and α are, in general, complex to permit phase differences between the translations in the x- and y-directions and the rotation.

The force and moment (coefficients) acting on the mth blade are given by

$$\hat{\boldsymbol{C}}_{F_m} = -\oint_{\mathscr{B}m} \hat{P}\boldsymbol{n}\, \mathrm{d}\tau = \boldsymbol{C}_F + \mathrm{Re}\{\boldsymbol{c}_F \mathrm{e}^{\mathrm{i}(\omega t + m\sigma)}\} + O(\epsilon^2) \tag{4.6}$$

and

$$\hat{C}_{M_m} = \oint_{\mathscr{B}m} \hat{P}\hat{\boldsymbol{R}}_p \cdot \mathrm{d}\boldsymbol{\tau} = C_M + \mathrm{Re}\{c_M \mathrm{e}^{\mathrm{i}(\omega t + m\sigma)}\} + O(\epsilon^2), \tag{4.7}$$

where the moment is taken about the moving pitching axis and $\hat{\boldsymbol{R}}_p$ extends from this axis to points on the moving blade surface. After some algebra, it follows that

$$\boldsymbol{c}_F = \boldsymbol{a} \times \boldsymbol{C}_F - \oint_B p_{\mathscr{B}} \boldsymbol{n}\, \mathrm{d}\tau + r_n(0)\, [\![P_B]\!]\, \boldsymbol{n}_B|_+ + r_n(0)\, [\![P_B]\!]\, \boldsymbol{n}_B|_- \tag{4.8}$$

and

$$c_M = \oint_B p_{\mathscr{B}} \boldsymbol{R}_p \cdot \mathrm{d}\boldsymbol{\tau} - r_n(0)\, [\![P_B]\!]\, (\boldsymbol{R}_{\mathrm{p}} \cdot \boldsymbol{\tau}_B)\,|_+ - r_n(0)\, [\![P_B]\!]\, (\boldsymbol{R}_p \cdot \boldsymbol{\tau}_B)|_-, \tag{4.9}$$

where $\boldsymbol{c}_F$ and c_M are the complex amplitudes of the unsteady force and moment respectively. The last two terms in (4.8) and (4.9) account for the concentrated loads due to shock motion, and they are evaluated at the mean positions of the shock roots.

5. Numerical approximation

For simplicity the numerical approximation will be outlined for transonic flow through a cascade of oscillating sharp-edged airfoils in which at most a single shock occurs in each blade passage. Thus unsteady phenomena associated with mean incidence and multiple shocks are omitted from present consideration. A numerical resolution of the linear variable-coefficient unsteady boundary-value problem is required over a single extended blade-passage region of finite extent. The unsteady differential equation, in this case (3.9), must be solved in continuous regions of the flow subject to boundary or jump conditions at the mean positions of the blade, wake and shock surfaces. Blade mean positions are prescribed, and the mean positions of wake (i.e. the downstream stagnation streamlines) and shock surfaces are determined as part of the steady solution. Finally, the unsteady, near-field numerical solution must be matched to far-field analytical solutions at finite distances (say $\xi = \xi_{\mp}$) upstream and downstream from the blade row. Since the unsteady numerical model along with its application to subsonic cascades has been described in detail in Caspar & Verdon (1981), here we describe primarily those modifications required for transonic applications.

In view of the stringent and often conflicting requirements placed on the construction of a computational mesh for cascade flows, we have adopted a two-step solution procedure. The basic approach is first to capture large-scale unsteady phenomena on a rectilinear-type cascade mesh of moderate density and then to determine a solution on a polar-type local grid of high density. The cascade mesh covers the extended-blade-passage solution domain, while the local mesh covers (and extends well beyond) a region of high velocity gradient; for example near a rounded leading edge in Verdon & Caspar (1982) or near a shock in the present study. The velocity-potential distribution as determined by the cascade-mesh solution provides outer boundary-condition information for the local calculation, and the solution to the unsteady boundary-value problem is taken to be the local solution in a region covered by a local mesh and the cascade solution elsewhere. At present the local solution is essentially a correction to the cascade solution, i.e. there is no iteration between the cascade and local calculations. Because of this it is necessary to choose a rather extensive local region.

The cascade mesh (see figure 2*a*) is composed of axial lines (ξ = constant) which are parallel to the blade row and tangential curves which are percentile averages of the upper and lower boundaries. This mesh facilitates the imposition of the cascade periodicity condition (3.6) and the matching of the analytical and numerical unsteady solutions at far field boundaries. However, it does not yield an accurate resolution

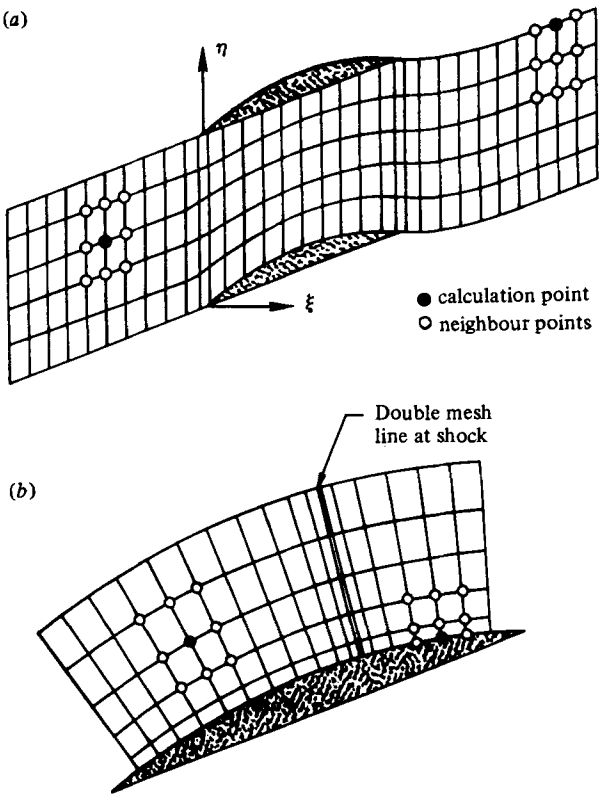

FIGURE 2. Calculation meshes for unsteady transonic cascade flow: (*a*) cascade mesh; (*b*) local mesh.

of the flow near rounded blade edges or near shocks, and it is not well suited for the accurate implementation of transonic differencing procedures. Thus in the present study a local mesh such as that shown in figure 2(*b*) is employed to resolve the flow in the vicinity of a normal shock and in the supersonic region lying adjacent to the blade surface and upstream of the shock. This mesh consists of radial and circumferential lines, normal and roughly parallel respectively to the reference blade surface. Two of the radial lines (hereinafter referred to as the upstream and downstream shock mesh lines) are positioned at the mean location of the shock foot so that information on the upstream and downstream side of the shock can be accurately represented. Hence the mean shock locus is currently approximated as being normal to the airfoil surface in the local unsteady calculation. The local mesh facilitates the imposition of the unsteady shock-jump conditions as well as the accurate implementation of the rotated and type-dependent transonic differencing strategies discussed below.

5.1. *Difference approximations*

Algebraic approximations to the various linear operators, which make up the unsteady boundary-value problem, are obtained using an implicit least-squares interpolation procedure. Thus consider a linear differential operator $\mathscr{L}$ which operates on a constant by multiplying that constant by q^0. An algebraic approximation $L\phi$ to $\mathscr{L}\phi$ at the mesh point Q_0 can be written in terms of the values of ϕ at Q_0 and

at certain neighbouring points Q_1, ..., Q_m, which together with Q_0 are called a neighbour set. This approximation can be expressed in the form

$$(\mathscr{L}\phi)_0 \approx (\mathrm{L}\phi)_0 \equiv q^0\phi_0 + \sum_{m=1}^{M} \beta_m(\phi_m - \phi_0), \tag{5.1}$$

where the difference coefficients β_m are evaluated in terms of a prescribed set of interpolating functions and a set of interpolating coefficients. The latter are determined by a weighted least-squares procedure. For the present application the neighbour sets are defined as shown in figure 2, i.e. in a 'centred' fashion for interior points and in a one-sided fashion for boundary points.

Following Murman & Cole (1971) for transonic applications the plan is to distinguish between regions of subsonic flow where the unsteady differential equation is elliptic and supersonic flow where it is hyperbolic, and to use a differencing scheme that is sensitive to its local character. To accomplish this we first apply the rotated differencing concept introduced by Jameson (1974). Thus at each point of the discrete domain the field equation is expressed in canonical form, i.e.

$$\mathscr{L}_0\phi = (\mathscr{L}_1 + \mathscr{L}_2)\phi, \tag{5.2}$$

where

$$\mathscr{L}_1\phi = A^2(1-M^2)\phi_{SS} = M^{-2}(1-M^2)(\Phi_\xi^2\phi_{\xi\xi} + 2\Phi_\xi\Phi_\eta\phi_{\epsilon\eta} + \Phi_\eta^2\phi_{\eta\eta}) \tag{5.3}$$

and

$$\mathscr{L}_2\phi = A^2\phi_{NN} + \ldots = M^{-2}[\Phi_\eta^2\phi_{\xi\xi} - 2\Phi_\xi\Phi_\eta\phi_{\xi\eta} + \Phi_\xi^2\phi_{\eta\eta}] + \ldots. \tag{5.4}$$

Here S and N are the local canonical coordinates, i.e. the Cartesian coordinates respectively aligned with and normal to, the local steady-flow direction, and ξ and η are the computational coordinates, i.e. the cascade axial and circumferential coordinates (see figure 1). The principal part of the unsteady differential equation is shown explicitly in (5.3) and (5.4), and the dots refer to the remaining terms. It is clear from (5.3) and (5.4) that the local character of the unsteady differential equation depends on the local steady Mach number, and it becomes a simple matter to construct a suitable type-dependent differencing scheme. The linear operator $\mathscr{L}_2$ is always approximated by a central-difference expression, but the difference approximation to the operator $\mathscr{L}_1$ will depend on the local steady Mach number and hence on the local type of the unsteady field equation. Thus we set

$$\mathscr{L}_1\phi|_{i,j} \approx \mathrm{L}_1\phi|_{i,j} \quad \text{if } M_{i,j} < 1 \tag{5.5}$$

and

$$\mathscr{L}_1\phi|_{i,j} \approx \mathrm{L}_1\phi|_{i-1,j} \quad \text{if } M_{i,j} > 1, \tag{5.6}$$

where the indices i and j refer to the axial and tangential lines respectively of the cascade mesh or to the radial and circumferential lines respectively of the local mesh, and L_1 is a central difference operator. Therefore at supersonic points the difference approximation to $\mathscr{L}_1\phi$ is retarded along the cascade tangential and the local circumferential mesh lines which are closely aligned with the mean-flow direction.

Unsteady shock phenomena are captured in the cascade calculation, i.e. the unsteady differential equation is approximated, using either (5.6) or (5.5) at the field points immediately upstream or downstream respectively of the mean shock location. Shocks are subsequently fitted into the local unsteady solution by imposing the jump condition (3.14) at the shock points on the downstream shock mesh line. The shock-jump condition is modelled using one-sided difference approximations (first-order accurate on the upstream or supersonic side and second-order accurate on the downstream or subsonic side) to evaluate the normal derivatives of the unsteady potential at the shock mean position. At those points on the downstream shock mesh

line at which the steady flow is continuous, the condition $[\![\phi]\!] = 0$ is imposed. To assist in evaluating the numerical solution procedure, a shock-capturing option has also been included in the local calculation. In this case the condition $[\![\phi]\!] = 0$ is imposed at all mesh points on the downstream shock mesh line.

5.2. *Solution procedure*

With the exception of supersonic field points and points on the upstream and downstream shock mesh lines, the systems of linear algebraic equations which approximate the linearized unsteady boundary values problem on the cascade and local meshes are constructed as described in Verdon & Caspar (1982). At a supersonic field point (i,j) the unsteady differential equation is approximated using neighbour sets centred at this point and at the adjacent upstream mesh point $(i-1,j)$. However, at points on the local upstream shock mesh line derivatives normal to the flow direction are evaluated only in terms of information provided along this mesh line to avoid crossing the shock. For points on the downstream shock mesh line the shock-jump (3.14) or the continuity $[\![\phi]\!] = 0$ condition is approximated as described above. This treatment leads to a block-pentadiagonal system of linear algebraic equations of the form

$$\left.\begin{aligned} \boldsymbol{C}_1\boldsymbol{\phi}_1+\boldsymbol{D}_1\boldsymbol{\phi}_2 &= \boldsymbol{F}_1, \\ \boldsymbol{A}_i\boldsymbol{\phi}_{i-2}+\boldsymbol{B}_i\boldsymbol{\phi}_{i-1}+\boldsymbol{C}_i\boldsymbol{\phi}_i+\boldsymbol{D}_i\boldsymbol{\phi}_{i+1}+\boldsymbol{E}_i\boldsymbol{\phi}_{i+2} &= \boldsymbol{F}_i \quad (2 \leqslant i \leqslant I-1), \\ \boldsymbol{B}_I\boldsymbol{\phi}_{i-1}+\boldsymbol{C}_I\boldsymbol{\phi}_I &= \boldsymbol{F}_I, \end{aligned}\right\} \tag{5.7}$$

where $\boldsymbol{\phi}_i$ is a vector of ϕ-values on the ith cascade axial or local radial mesh line, and the submatrices $\boldsymbol{A}_i$, $\boldsymbol{B}_i$, $\boldsymbol{C}_i$, $\boldsymbol{D}_i$ and $\boldsymbol{E}_i$ are sparse, being mostly scalar-tridiagonal. Note that, with the exception of the points on the downstream side of a fitted shock, $\boldsymbol{A}_i \equiv 0$ at subsonic points and $\boldsymbol{E}_i \equiv 0$. With this structure the system of equations (5.7) can be solved directly and efficiently using Gaussian elimination.

6. Numerical examples

The foregoing analysis has been applied to cascades of vibrating sharp-edged double-circular-arc (DCA) airfoils operating at high subsonic inlet Mach number. The mean location of the zeroth or reference blade surface is defined by

$$y_\pm(x) = \begin{cases} \operatorname{sgn}(H_\pm)\{|H_\pm|-R_\pm+[R_\pm^2-(x-0.5)^2]^{\frac{1}{2}}\} & \text{for } H_\pm \neq 0, \\ 0 & \text{for } H_\pm = 0, \end{cases} \tag{6.1}$$

where $0 \leqslant x \leqslant 1$, H is the y-coordinate of the surface at midchord, $R = \frac{1}{2}|H|^{-1}(H^2+0.25)$ is the radius of curvature of the surface, $\operatorname{sgn}(H) = \pm 1$ for $H \gtrless 0$, and the subscripts $+$ or $-$ refer to the upper or lower surfaces of the blade. For simplicity we will present only results for a single DCA configuration: a staggered (with $\Theta = 45°$) array with unit gap/chord ratio ($G = 1$) and consisting of 5 % thick flat-bottomed DCA blades (i.e. $H_+ = 0.05$, $H_- = 0$). In addition, for purposes of comparison, results will also be presented for a similar array (i.e. $\Theta = 45°$, $G = 1$) of flat-plate ($H_\pm = 0$) airfoils. For the flat-plate cascade the steady Mach number will be constant throughout the field, and hence there will be no coupling between the steady and unsteady flows.

The unsteady solutions presented here have been determined on a cascade mesh extending one axial chord upstream and downstream from the blade row and, for those cases in which a normal shock emanates from the suction surface of each blade, on a local mesh extending from 10–90 % of blade chord along the suction surface of

the reference blade and outward from this surface to well beyond the end of the shock. A cascade mesh consisting of 100 axial lines, 44 of which intersect the blade surfaces, and 30 tangential lines was employed. The local mesh consisted of 61 radial lines and 11 circumferential lines. Variable mesh spacings were used in both the cascade and local calculations, with cascade tangential and local circumferential lines concentrated near blade surfaces, cascade axial lines concentrated near blade edges, and local radial lines concentrated near shocks. First-harmonic unsteady pressure-difference $\Delta p(x)$ distributions, where

$$\Delta p(x) = p_{\mathscr{B}}(x, y_-) - p_{\mathscr{B}}(x, y_+) \quad \text{for } 0 \leqslant x \leqslant 1, \tag{6.2}$$

shock-foot displacements $r_n(0)$ and unsteady moment coefficients c_M will be presented for blades undergoing pure torsional motions (with $\alpha = 1, 0$) about their midchord points (X_p, $Y_p = 0.5, 0$) at prescribed frequencies ω and interblade phase angles σ. The stability of such motions is governed by the out-of-phase (with blade displacement) component of the unsteady moment. Thus if $\mathrm{Im}\{c_M\} < 0$, the airstream tends to suppress a pure torsional motion, and hence this motion will be stable according to linear theory.

6.1. *Steady Mach-number distributions*

Full potential steady flows through the DCA cascades have been determined on similar but coarser cascade and local meshes using the finite-area numerical approximation developed by Caspar (1983). In each case the mean inlet Mach number $M_{-\infty}$ is prescribed and the requirements

$$\boldsymbol{V} \cdot \mathrm{d}\boldsymbol{\tau}|_{B-} = -\boldsymbol{V} \cdot \mathrm{d}\boldsymbol{\tau}|_{B+} \quad \text{for } x = 0, 1 \tag{6.3}$$

are imposed at blade leading (unique incidence condition) and trailing (Kutta condition) edges to uniquely specify the steady flow field. It should be noted that with Caspar's procedure the steady differential equation is solved in conservative form (see §2.1) and shocks are captured. Although it would be preferable to use a steady solution with a fitted shock for the present application, it appears that steady information in the vicinity of a shock has been determined with sufficient accuracy to define the mean shock location and to permit the imposition of shock-jump conditions in the unsteady calculation.

Predicted steady surface Mach-number distributions for the example DCA configuration are shown in figure 3. The prescribed inlet Mach numbers are 0.5, 0.7, 0.8, and 0.9 and the calculated exit Mach numbers M_∞ are 0.43, 0.57, 0.62 and 0.65 respectively. The corresponding inlet flow angles $\Omega_{-\infty}$ are 49.0°, 49.2°, 49.4° and 49.6° respectively, and in each case the exit flow angle Ω_∞ is 43.0°. The steady flows at $M_{-\infty} = 0.5$, $M_{-\infty} = 0.7$ and $M_{-\infty} = 0.8$ are entirely subsonic, with peak suction-surface Mach numbers of 0.561, 0.804 and 0.941 occurring at respectively 40.8, 38.5 and 36.7 % of blade chord downstream from the leading edge. The steady flow is transonic for $M_{-\infty} = 0.9$, with the supersonic region extending from 18.5 to 52.5 % of blade chord along the suction surface and terminating at a shock. The Mach numbers at the foot of the shock are 1.193 on the upstream or supersonic side and 0.871 on the downstream or subsonic side.

6.2. *Unsteady response predictions*

Numerical results will be presented for cascades of DCA and flat-plate airfoils undergoing out-of-phase ($\sigma = 180°$) or in-phase ($\sigma = 0°$) torsional vibrations at low ($\omega = 0.1$) through moderate (up to $\omega = 1.0$) frequencies and at the inlet Mach numbers indicated in figure 3. Particular emphasis will be placed on the unsteady response

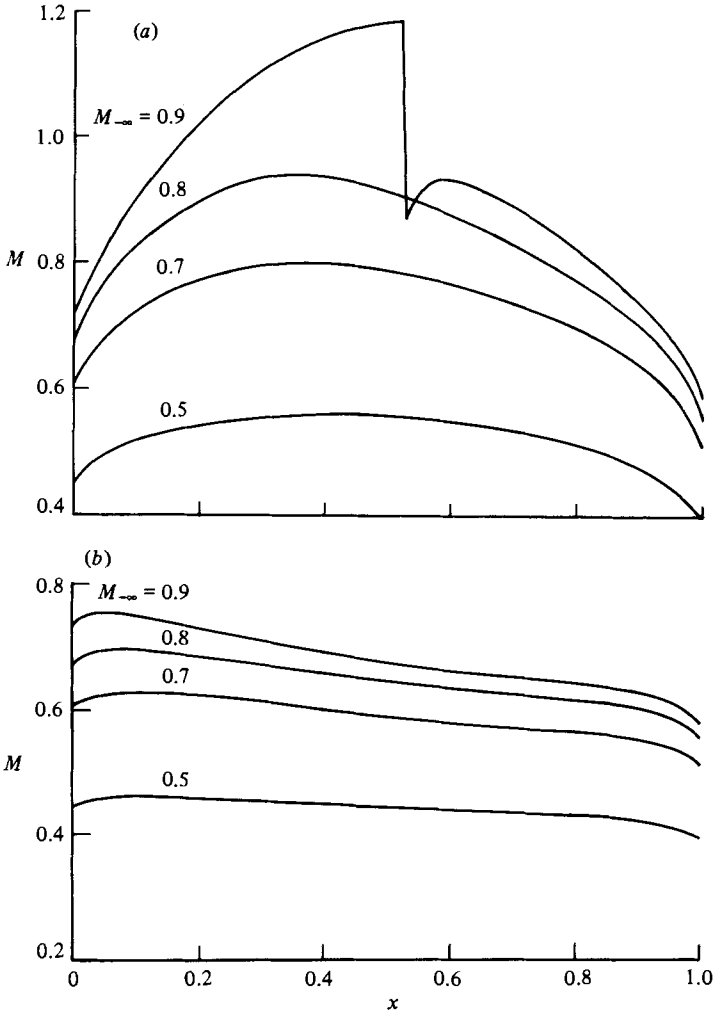

FIGURE 3. Steady surface Mach-number distributions for the example DCA cascade: (*a*) suction surface; (*b*) pressure surface.

predictions for the transonic flows at $M_{-\infty} = 0.9$, and the highest frequency considered is the most representative one for turbomachinery flutter applications. The inlet and exit Mach numbers differ substantially for the staggered DCA configuration, and this difference effects the overall character of the unsteady flow. For example, at $M_{-\infty} = 0.9$, unit-frequency out-of-phase torsional vibrations of both the staggered DCA ($M_\infty = 0.65$) and flat-plate ($M_\infty = 0.9$) cascades are superresonant. However, acoustic energy only propagates in the far-upstream direction for the DCA array because the waves travelling downstream at the lower exit Mach number attenuate with increasing distance from the blade row.

A comparison of the results shown in figures 4–6 illustrates several features of the numerical solution procedure. Cascade and combined (i.e. cascade and local) mesh response predictions for the staggered DCA configuration operating at an inlet Mach number of 0.9 are shown in figures 4 and 5 respectively. These results have been determined by shock capture, i.e. the field equation has been solved across the shock in the cascade calculation and the continuity condition $[\![\phi]\!] = 0$ has been imposed on

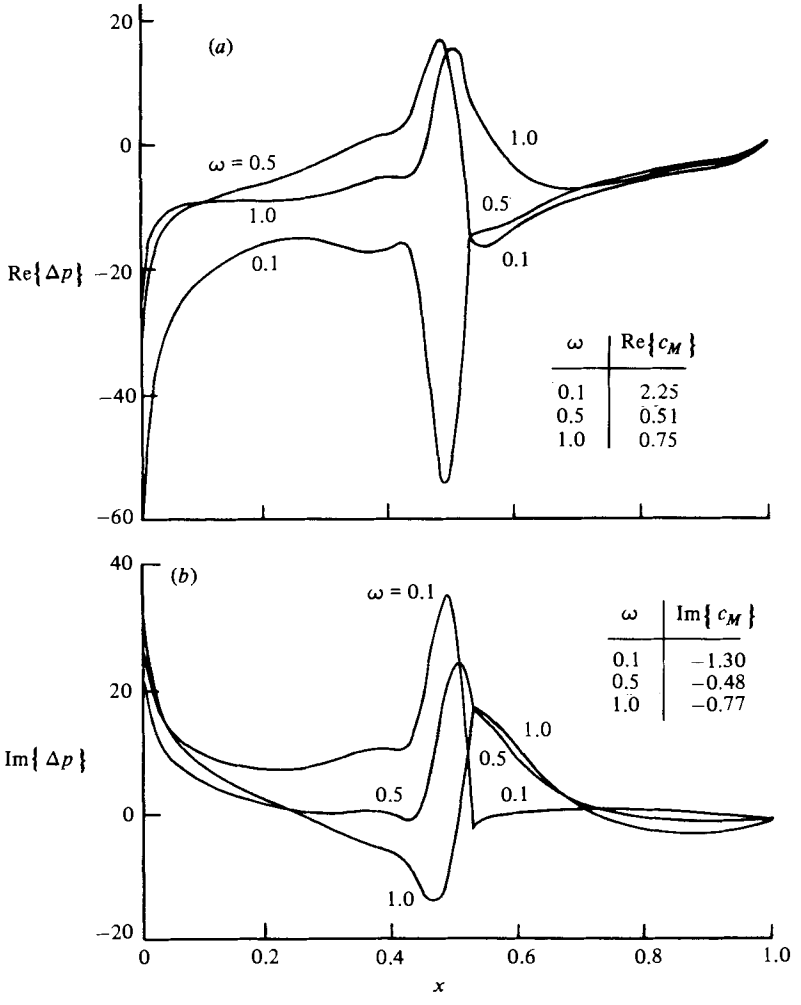

FIGURE 4. Cascade mesh-response predictions for torsional blade vibrations of the example DCA cascade; $M_{-\infty} = 0.9$, $\sigma = 180°$: (*a*) in-phase component (real part) of the unsteady response; (*b*) out-of-phase component (imaginary part) of the unsteady response.

the downstream shock mesh line in the local calculation, and they clearly illustrate the need for the local unsteady analysis to resolve the flow through a staggered transonic cascade. The errors associated with the cascade calculation occur because this mesh is highly skewed and, as a result, a number of axial mesh lines cross the normal shock. The combined mesh solutions shown in figure 5 indicate the significant improvement in resolution near the shock that can be achieved with the local mesh calculation. The pressure-difference predictions shown in figure 6 have been determined by imposing the shock-jump condition (3.14) in the local calculation. The continuous (figure 5) and discontinuous (figure 6) surface-pressure distributions are identical upstream, but differ substantially downstream, of the shock discontinuity. The results shown in figures 5 and 6 reveal the strong impact of shock displacement on the first-harmonic surface-pressure response, particularly at low vibration frequency.

The effect of frequency on the response to out-of-phase torsional blade vibrations of the staggered DCA and flat-plate cascades operating at $M_{-\infty} = 0.9$ is illustrated in figures 6 and 7. These blade motions are subresonant for $\omega = 0.1$ and 0.25, and

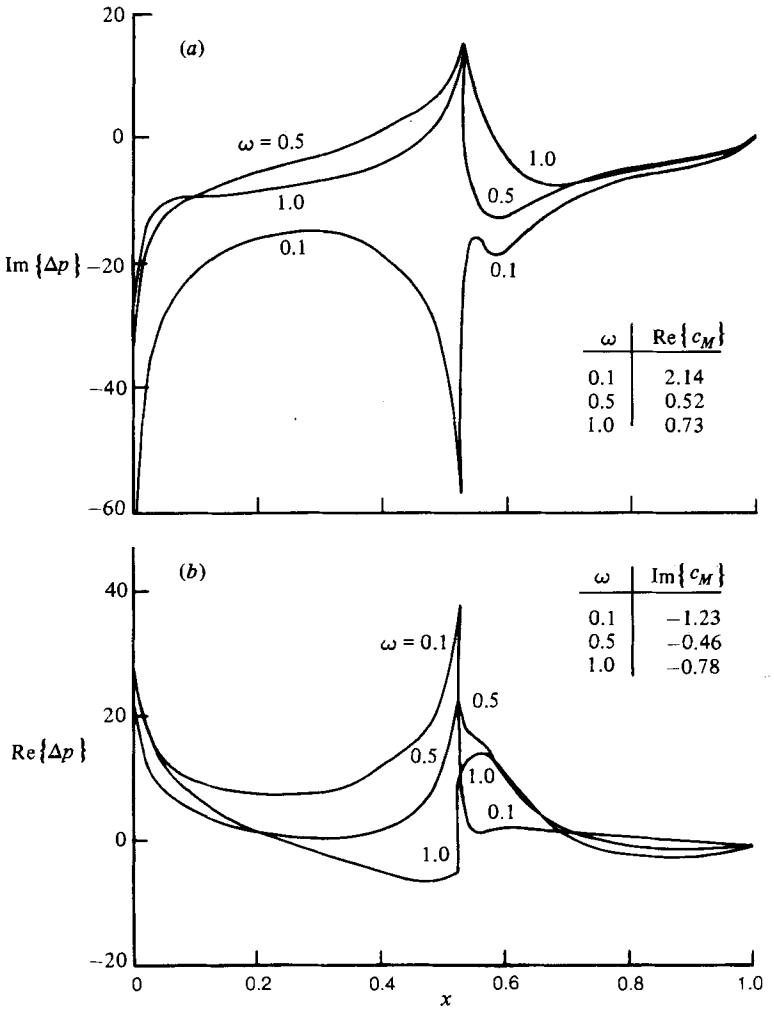

FIGURE 5. Cascade plus local mesh-response predictions for torsional blade vibrations of the example DCA cascade: unsteady solutions determined by shock capture; $M_{-\infty} = 0.9$, $\sigma = 180°$: (*a*) and (*b*) as in figure 4.

superresonant for $\omega = 0.5$, 0.75 and 1.0. For the DCA cascade the complex shock displacement $r_n(0)$ along the blade surface leads the blade rotational displacement α by an angle greater than 90° for $\omega = 0.1$ and 0.25 and less than 90° for $\omega = 0.5$, 0.75 and 1.0. Hence the instantaneous location of the shock foot will generally be upstream of its mean position for the two lower frequencies and downstream of its mean position for the three higher frequencies, when the blade is displaced nose-down from its mean position. For the examples considered in figure 6 one effect of including the shock displacement in the local solution (see also figure 5) is a decrease in the imaginary part of the unsteady pressure difference downstream of the shock, and hence a decrease in the out-of-phase moment, i.e. stability enhancement. However, the anharmonic component of the unsteady pressure produced by the shock motion partially compensates for this effect. The steady pressure jump across the foot of the shock is positive ($[\![P_B]\!] = 0.593$), the shock mean position is slightly downstream of the torsional axis ($\boldsymbol{R}_p \cdot \boldsymbol{\tau}_B = -0.025$), and the out-of-phase component of the shock

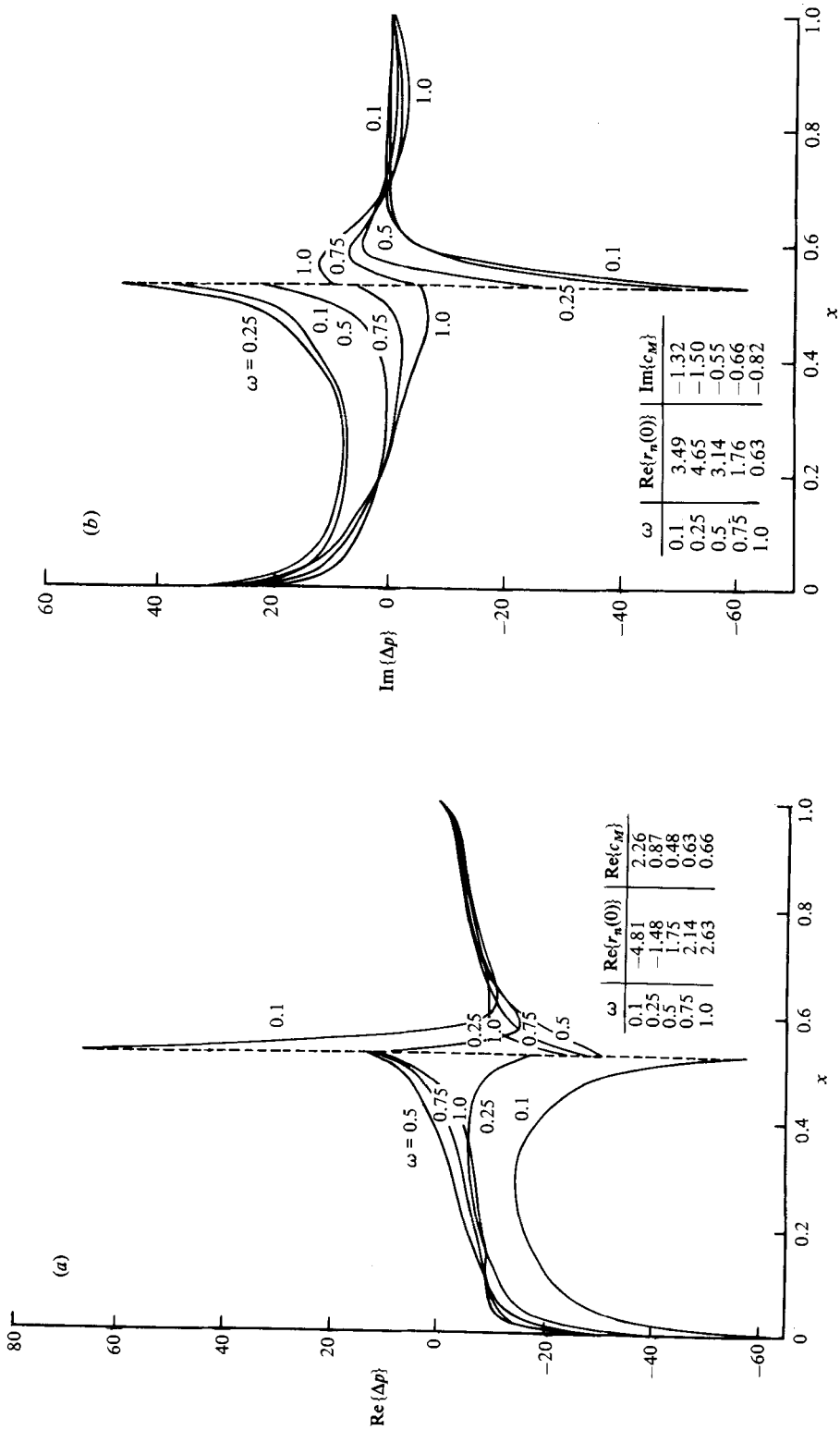

FIGURE 6. Effect of frequency on the unsteady response due to torsional blade vibrations of the DCA cascade; $M_{-\infty} = 0.9$, $\sigma = 180°$: (*a*) and (*b*) as in figure 4.

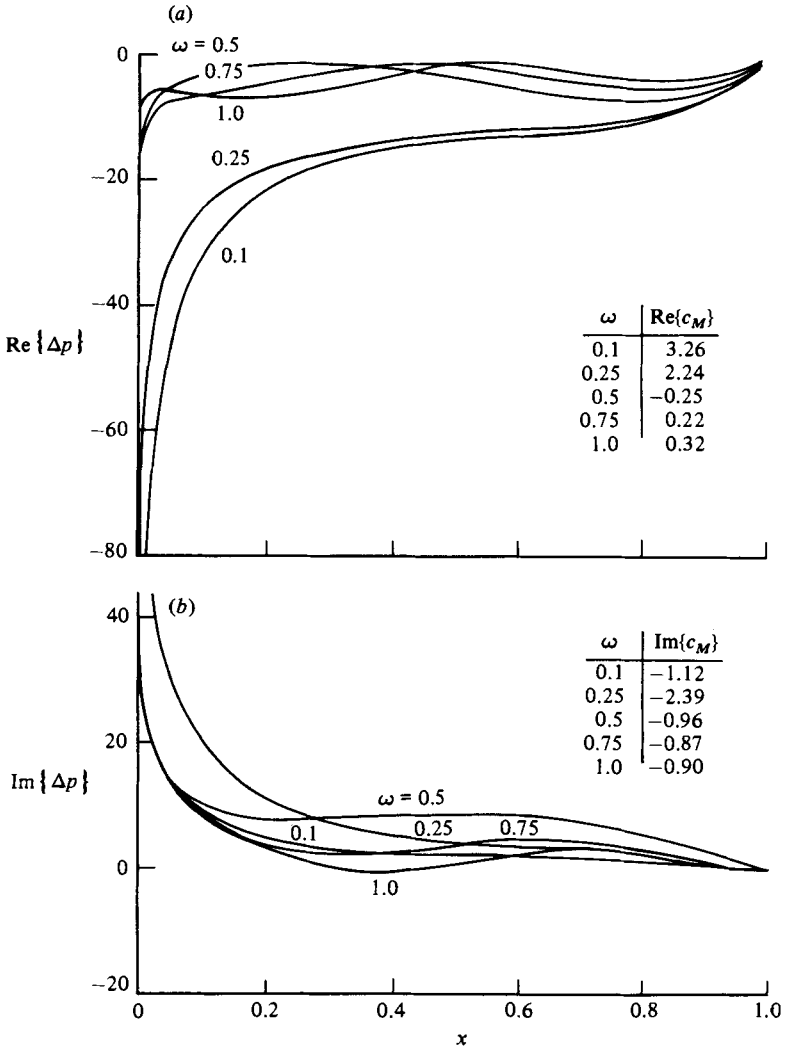

FIGURE 7. Effect of frequency on the unsteady response due to torsional blade vibrations of the example flat-plate cascade; $M_{-\infty} = 0.9$, $\sigma = 180°$: (*a*) and (*b*) as in figure 4.

displacement is positive ($\mathrm{Im}\{r_n(0)\} > 0$). Therefore the anharmonic component of the unsteady pressure produces a small but positive or counterclockwise imaginary moment (see (4.9)) which tends to amplify the blade motion. However, for the blade motions considered in figure 6 the net effect of shock displacement is a stabilizing one. A comparison of the DCA results in figure 6 with those for the flat-plate cascade in figure 7 reveals the dramatic influence of steady/unsteady interactions on the low through moderate frequency unsteady response at high subsonic inlet Mach number. The moment predictions for the staggered DCA configuration in figure 6(*b*) and for the flat-plate configuration in figure 7 indicate that the stability margin for out-of-phase torsional vibrations is significantly reduced as the frequency increases through a resonance condition.

The effect of frequency on the response to in-phase torsional blade vibrations of staggered DCA and flat-plate cascades is illustrated in figures 8 and 9. The motions

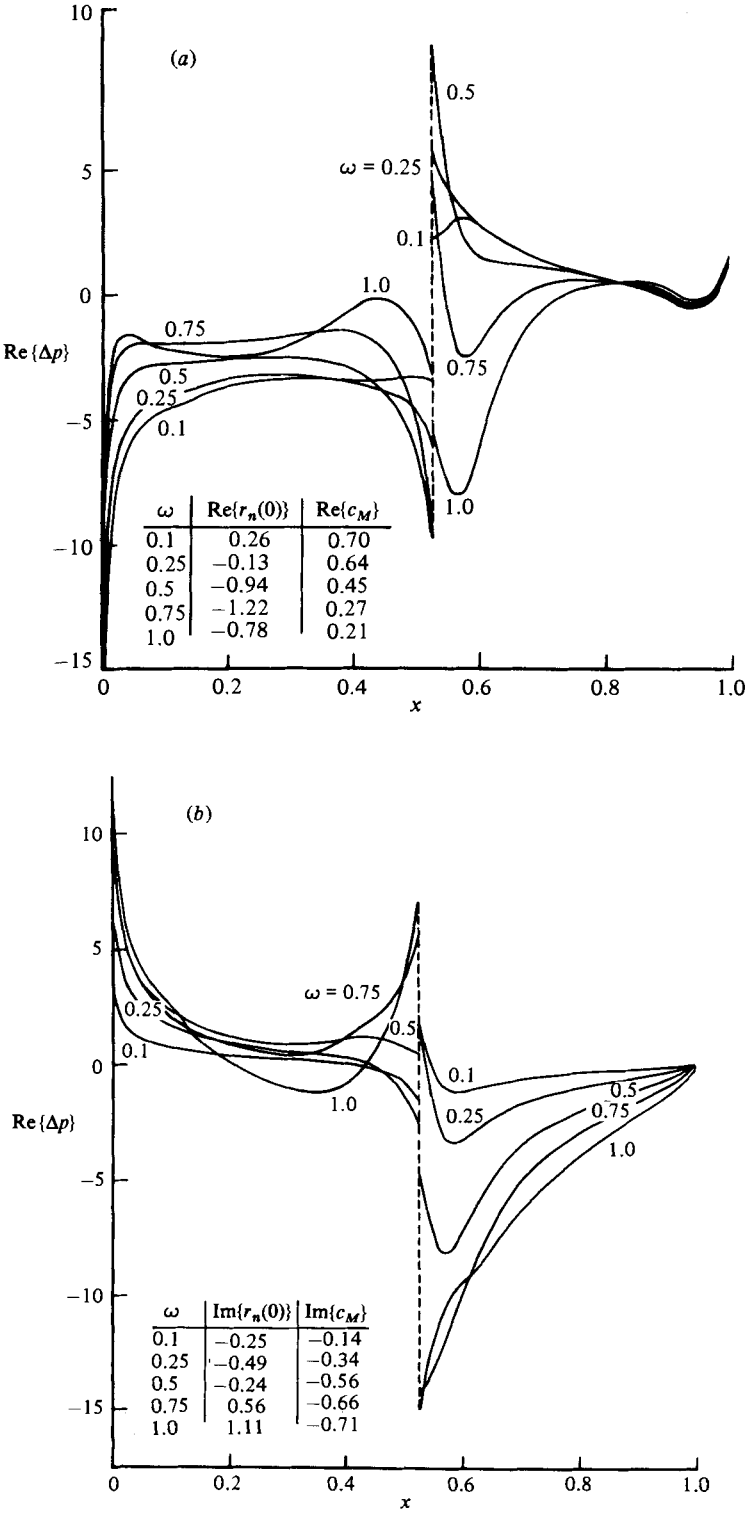

FIGURE 8. Effect of frequency on the unsteady response due to in-phase ($\sigma = 0°$) torsional vibrations of the DCA cascade; $M_{-\infty} = 0.9$: (*a*) and (*b*) as in figure 4.

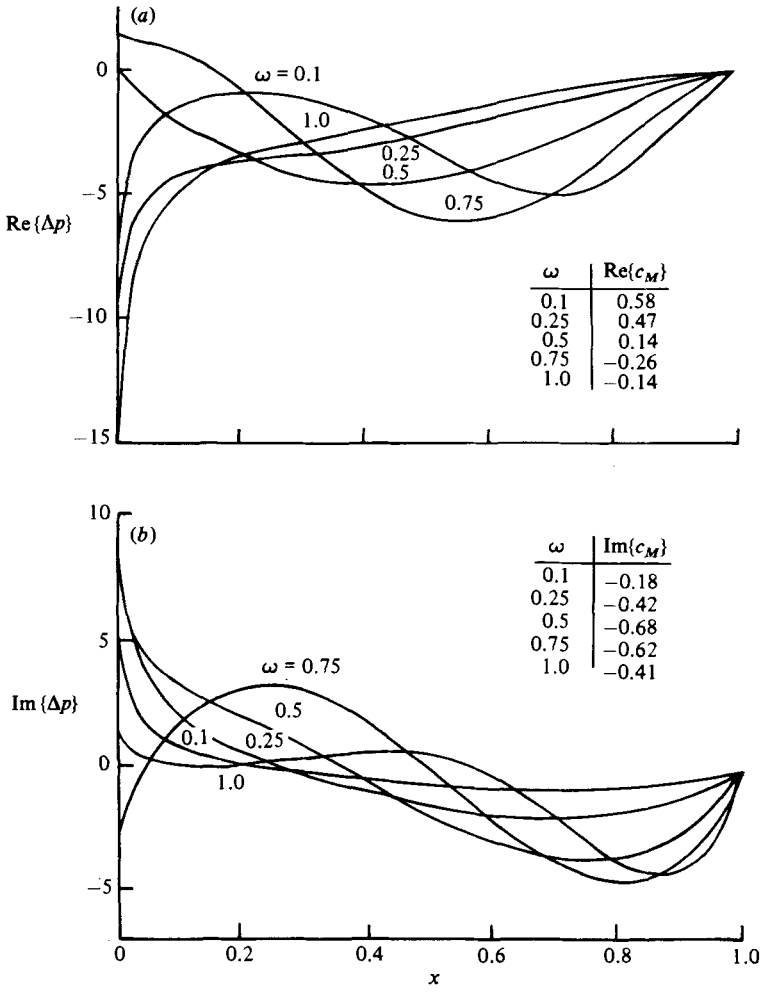

FIGURE 9. Effect of frequency on the unsteady response due to in-phase torsional blade vibrations of the flat-plate cascade; $M_{-\infty} = 0.9$: (*a*) and (*b*) as in figure 4.

considered here are superresonant, with acoustic energy propagating away from the blade row in both the far-upstream and far-downstream directions. The amplitudes of the complex response coefficients for the in-phase torsional vibrations depicted in figures 8 and 9 are generally smaller than those for out-of-phase torsional vibrations depicted in figures 6 and 7, particularly at the two lower frequencies $\omega = 0.1$ and 0.25, where the in-phase vibrations are superresonant and the out-of-phase vibrations are subresonant. For the staggered DCA cascade operating at $M_{-\infty} = 0.9$ the complex shock displacement $r_n(0)$ lags the blade rotational displacement for $\omega = 0.1$, 0.25 and 0.5, and leads the rotational displacement for $\omega = 0.75$ and 1.0. Thus the out-of-phase component $\mathrm{Im}\{r_n(0)\}$ of the shock displacement is negative at the three lower frequencies and positive at the two higher frequencies. Since the mean shock location is slightly aft of midchord, the concentrated load due to shock motion produces a small stabilizing moment for $\omega = 0.1$, 0.25 and 0.5 and a small destabilizing moment for $\omega = 0.75$ and 1.0. However, owing to its influence on the harmonic surface-pressure response, the net effect of the shock motion is a destabilizing one at the three lower frequencies and a stabilizing one at the two higher frequencies. The stability margin

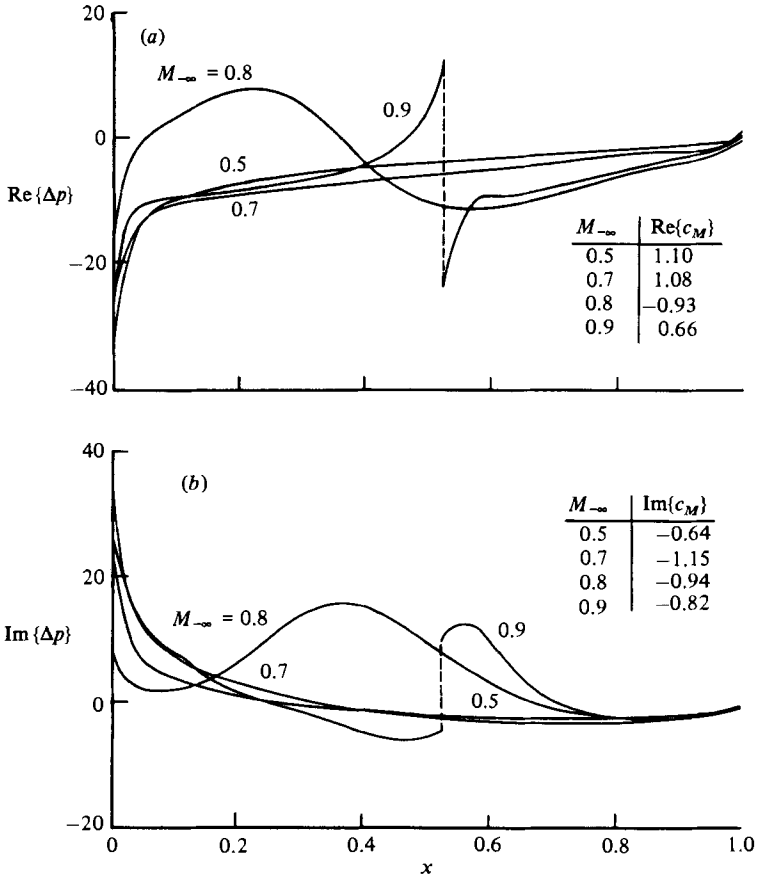

FIGURE 10. Effect of Mach number on the unit-frequency response due to out-of-phase ($\sigma = 180°$) torsional blade vibrations of the DCA cascade: (*a*) and (*b*) as in figure 4.

for in-phase torsional vibrations of the DCA cascade tends to increase with increasing frequency (figure 8*b*), but this is not the case for the flat-plate cascade (figure 9) where the moment ($-\mathrm{Im}\{c_M\}$) resisting the blade motion is greater at $\omega = 0.5$ than it is at the other frequencies.

The effect of Mach number on the unit-frequency response to out-of-phase and in-phase torsional vibrations of the DCA and flat-plate cascades is illustrated in figures 10–13. A comparison of these DCA and flat-plate results again reveals the substantial impact of mean-flow gradients on unsteady response, particularly at high-subsonic inlet Mach number. Recall that at $M_{-\infty} = 0.5$, 0.7 and 0.8 the flow through the DCA cascade is everywhere subsonic, while at $M_{-\infty} = 0.9$ it is transonic with a shock emanating from the suction surface of each blade. The out-of-phase motions of the DCA cascade are subresonant at $M_{-\infty} = 0.5$ and 0.7, and superresonant at the two higher Mach numbers, while the out-of-phase motions of the flat-plate cascade are subresonant at $M_{-\infty} = 0.5$, 0.7 and 0.8, and superresonant at $M_{-\infty} = 0.9$. For each cascade the out-of-phase motion at $M_{-\infty} = 0.8$ is close to a resonance condition, and as a result accurate response predictions are difficult to achieve. The in-phase motions of both the DCA and flat-plate cascades are superresonant. The unsteady pressure-difference distributions for the out-of-phase vibrations of the DCA (figure 10) and flat-plate (figure 11) cascades are very similar for $M_{-\infty} = 0.5$ and 0.7, but differ

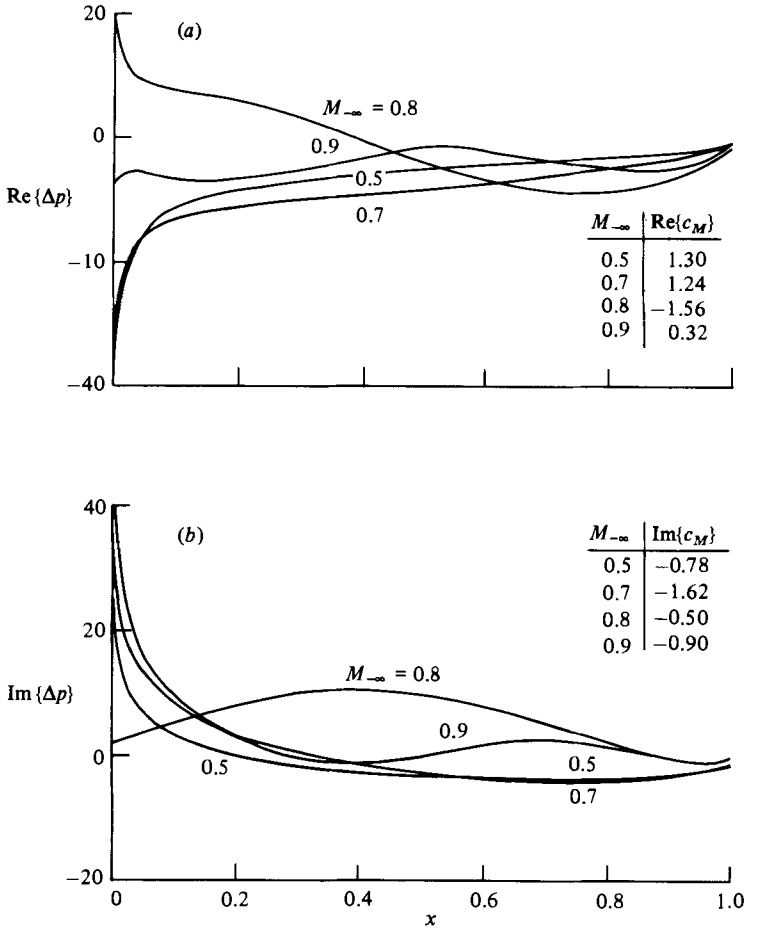

FIGURE 11. Effect of Mach number on the unit-frequency response due to out-of-phase torsional blade vibrations of the flat-plate cascade: (*a*) and (*b*) as in figure 4.

substantially for $M_{-\infty} = 0.8$ and 0.9. The differences at $M_{-\infty} = 0.8$ are primarily due to the different character of the unsteady motions (i.e. superresonant *vs.* subresonant) and to the near-resonance operation of each cascade. At the highest Mach number the differences in the DCA and flat-plate unsteady pressure-difference distributions are clearly due to the transonic and shock-motion phenomena associated with the DCA configuration. For the four inlet Mach numbers considered, the stability margin for the out-of-phase torsional vibrations is the lowest at $M_{-\infty} = 0.5$ for the DCA cascade and at $M_{-\infty} = 0.8$ for the flat-plate cascade. The unsteady pressure-difference distributions for the in-phase vibrations of the DCA and flat-plate cascades are again similar for $M_{-\infty} = 0.5$ and 0.7, differ somewhat for $M_{-\infty} = 0.8$ and differ substantially for $M_{-\infty} = 0.9$. The differences at $M_{-\infty} = 0.8$ can be attributed to the relatively large mean Mach-number gradients which occur along the suction surface and upstream of midchord of each DCA blade, while those at $M_{-\infty} = 0.9$ are due to the transonic phenomena occurring in the DCA cascade. The in-phase torsional stability margin for both the DCA and flat plate cascades is lowest at $M_{-\infty} = 0.5$.

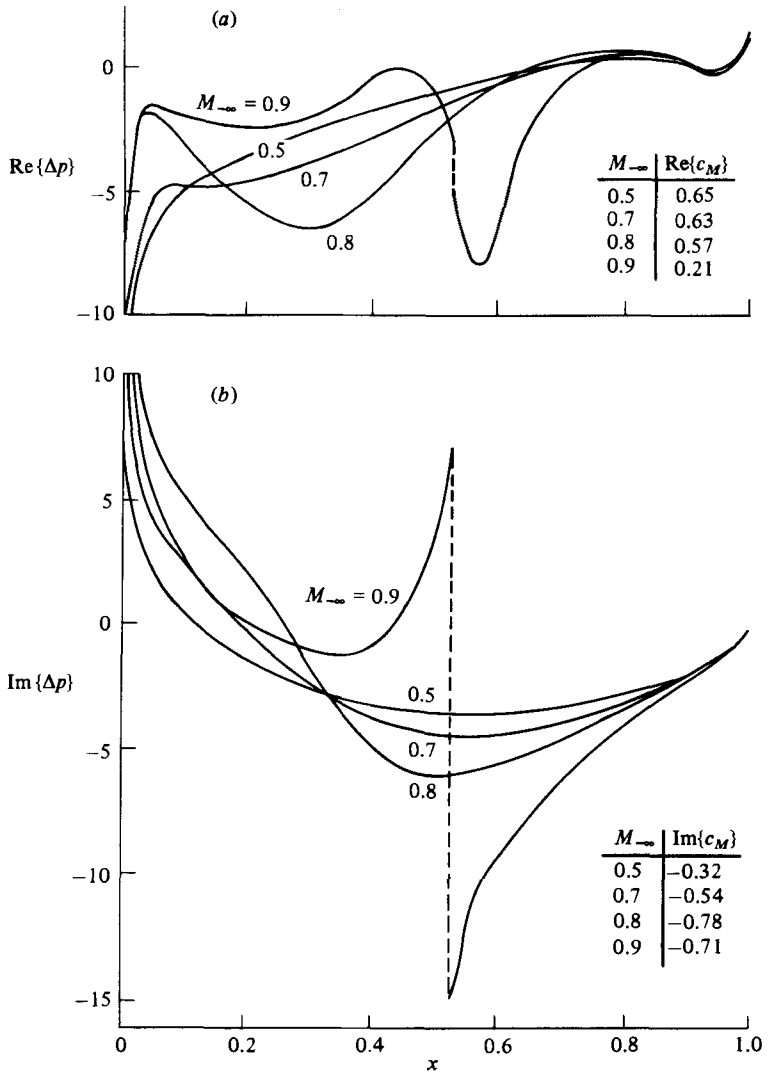

FIGURE 12. Effect of Mach number on the unit-frequency response due to in-phase ($\sigma = 0°$) torsional blade vibrations of the DCA cascade: (*a*) and (*b*) as in figure 4.

7. Concluding remarks

A linearized unsteady aerodynamic analysis has been developed for turbomachinery aeroelastic applications. Here the unsteady flow is produced by the small-amplitude (infinitesimal) harmonic vibrations of the blades of a two-dimensional cascade operating in an inviscid subsonic or transonic flow with embedded shocks. The unsteady potential is determined as the solution of a linear variable-coefficient boundary-value problem in which surface conditions are imposed at the mean positions of blade, wake and shock surfaces, and the variable coefficients depend on the underlying full potential, mean or steady flow. The local character of the unsteady differential equation (i.e. elliptic or hyperbolic) depends on the local steady Mach number, and the unsteady potential is discontinuous at shock mean positions. Shock displacement and hence the concentrated loads produced by this displacement are

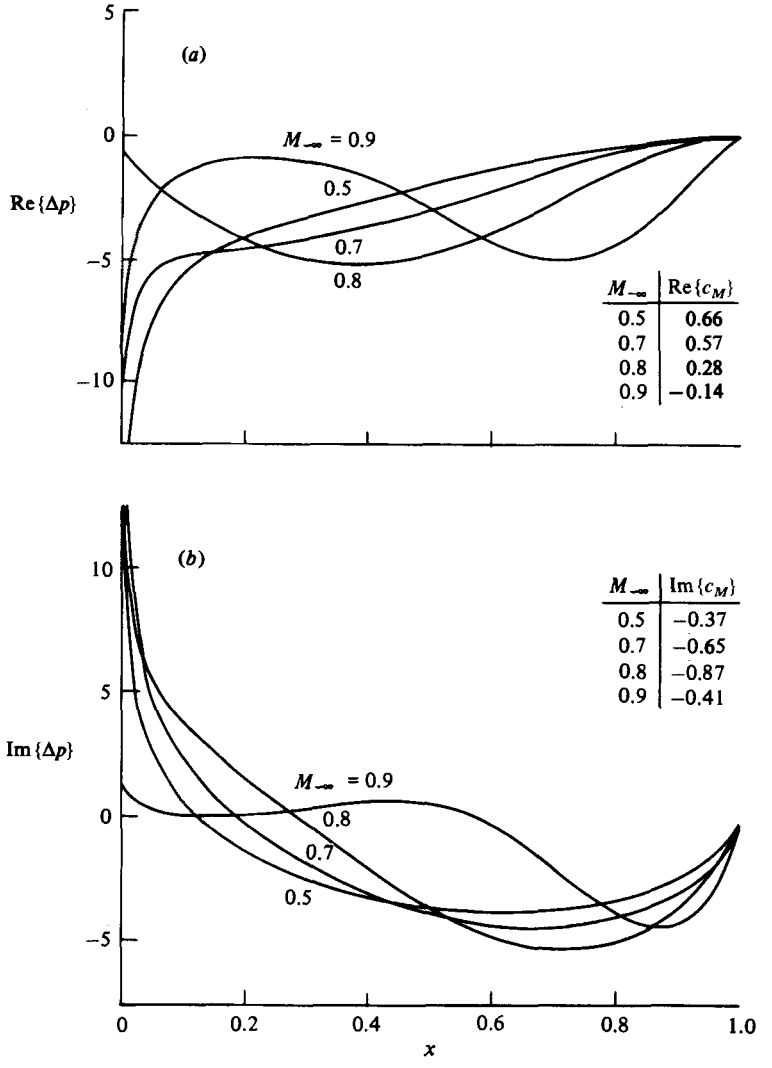

FIGURE 13. Effect of Mach number on the unit-frequency response due to in-phase torsional blade vibrations of the flat-plate cascade: (*a*) and (*b*) as in figure 4.

proportional to the discontinuity in the unsteady potential. This analysis is intended for application at the reduced frequencies of interest for turbomachinery flutter applications (i.e. $\omega = O(1)$) and includes the effects of real blade geometry and mean blade loading as well as the effects of transonic Mach numbers and shock motions within the framework of a linear frequency-domain formulation. It is therefore believed to represent an important advance over the classical linearized analyses currently employed in turbomachinery aeroelastic studies and over the time-linearized unsteady transonic analyses that have been developed for fixed-wing applications.

The unsteady solutions presented in this paper have been determined by applying an implicit least-squares finite-difference approximation on cascade and local grids. Numerical examples have been provided to establish confidence in the unsteady analysis, especially at high reduced frequency, and to illustrate the strong impact of non-uniform steady flow on the unsteady response at high subsonic and transonic

Mach numbers. Particular emphasis has been placed on evaluating the effects of shock motions. Such motions must be included to achieve a uniformly valid first-order transonic solution. In future work efforts should be undertaken to extend the range of application and to improve the accuracy of the unsteady numerical approximation. In particular, the local calculation should be applied on a mesh that wraps around a rounded leading edge and extends along the lower surface of the reference blade so that mean incidence effects and multiple shock phenomena can be analysed simultaneously. In addition, mean-flow equipotential and streamlines should be used as local mesh lines in the vicinity of a shock to permit a more accurate resolution of unsteady shock phenomena, and an iterative procedure should be used to match the cascade and local solutions properly. Finally, detailed parametric studies should be conducted to provide a more complete understanding of the effects of blade geometry and loading, blade-vibration mode and frequency, and shock motion, on the unsteady aerodynamic response, and hence on the aerodynamic stability of cascades operating at transonic Mach numbers.

This research was supported by NASA Lewis Research Center Contract NAS3-23696. This support and the advice and assistance provided by Dr John J. Adamczyk, NASA Program Manager for the contract, are gratefully acknowledged.

REFERENCES

ARIS, A. 1962 *Vectors, Tensors and the Basic Equations of Fluid Mechanics.* Prentice-Hall.

ATASSI, H. & AKAI, T. J. 1978 Effect of blade loading and thickness on the aerodynamics of oscillating cascades. *AIAA 16th Aerospace Sciences Meeting; Paper* 78-227.

CARTA, F. O. 1983 Unsteady aerodynamics and gapwise periodicity of oscillating cascaded airfoils. *Trans. ASME* A: *J. Engng for Power* **105**, 565.

CARUTHERS, J. E. 1981 Aerodynamic analysis of cascaded airfoils in unsteady rotational flow. In *Proc. 2nd Intl Symp. on Aeroelasticity in Turbomachines* (ed. P. Suter), pp. 31–64. Juris, Zurich.

CASPAR, J. R. 1983 Unconditionally stable calculation of transonic potential flow through cacades using an adaptive mesh for shock capture. *Trans. ASME* A: *J. Engng for Power* **105**, 504.

CASPAR, J. R. & VERDON, J. M. 1981 Numerical treatment of unsteady subsonic flow past an oscillating cascade. *AIAA J.* **19**, 1531.

EHLERS, F. E. & WEATHERILL, W. H. 1982 A harmonic analysis method for unsteady transonic flow and its application to the flutter of airfoils. *NASA CR* 3537.

FUNG, K. Y., YU, N. J. & SEEBASS, R. 1978 Small unsteady perturbations in transonic flows. *AIAA J.* **16**, 815.

GOLDSTEIN, M. E. 1979 Turbulence generated by the interaction of entropy fluctuations with non-uniform mean flows. *J. Fluid Mech.* **93**, 209.

GOLDSTEIN, M. E., BRAUN, W. ADAMCZYK, J. J. 1977 Unsteady flow in a supersonic cascade with strong in-passage shocks. *J. Fluid Mech.* **83**, 569.

HOUNJET, M. H. L. 1981 Transonic panel method to determine loads on oscillating airfoils with shocks. *AIAA J.* **19**, 559.

HUNT, J. C. R. 1973 A theory of turbulent flow round two-dimensional bluff bodies. *J. Fluid Mech.* **61**, 225.

JAMESON, A. 1974 Iterative solution of transonic flows over airfoils and wings including flows at Mach 1. *Commun. Pure Appl. Maths* **27**, 283.

MCNALLY, W. D. & SOCKOL, P. M. 1981 Computational methods for internal flows with emphasis on turbomachinery. *NASA Tech. Memo.* 82764.

MURMAN, E. H. & COLE, J. D. 1971 Calculation of plane steady transonic flows. *AIAA J.* **9**, 114.

TIJDEMAN, H. 1977 Investigations of the transonic flow around oscillating airfoils. *Natl Aerosp. Lab. Rep.* NLR TR 77090-U.

TIJDEMAN, H. & SEEBASS, R. 1980 Transonic flow past oscillating airfoils. *Ann. Rev. Fluid Mech.* **12**, 181.

VERDON, J. M. & CASPAR, J. R. 1980 Subsonic flow past an oscillating cascade with finite mean flow deflection. *AIAA J.* **18**, 540.

VERDON, J. M. & CASPAR, J. R. 1982 Development of a linear unsteady aerodynamic analysis for finite-deflection subsonic cascades. *AIAA J.* **20**, 1259.

WHITEHEAD, D. S. 1980 Unsteady aerodynamics in turbomachinery. *Special Course on Unsteady Aerodynamics; AGARD Rep.* 679.

WHITEHEAD, D. S. & GRANT, R. J. 1981 Force and moment coefficients for high deflection cascades. In *Proc. 2nd Intl Symp. on Aeroelasticity in Turbomachines* (ed. P. Suter), pp. 85–127. Juris, Zurich.

WHITHAM, G. B. 1974 *Linear and Nonlinear Waves.* Wiley.

WILLIAMS, M. H. 1979 Linearization of unsteady transonic flows containing shocks. *AIAA J.* **17**, 394.